ACS APPLIED MATERIALS & INTERFACES

www.acsami.org

Research Article

Self-Rolling of Monolayer Graphene for Ultrasensitive Molecular Sensing

Zhe Ma, Ziao Tian, Xing Li, Chunyu You, Yalan Wang, Yongfeng Mei,* and Zengfeng Di*

Cite This: https://doi.org/10.1021/acsami.1c12592

Read Online

ACCESS | Metrics & More | Article Recommendations | Supporting Information

ABSTRACT: The controllable manipulation of graphene to create three-dimensional (3D) structures is an intriguing approach for favorably tuning its properties and creating new types of 3D devices. However, due to extremely low bending stiffnesses, it is rather challenging to construct monolayer graphene into stable 3D structures. Here, we demonstrate the stable formation of monolayer graphene microtubes with accompanying pre-patterned strain layers. The diameter of graphene microtubes can be effectively tuned by changing the thickness of the strain layers. Benefiting from a high surface-to-volume ratio of the tubular geometry, the 3D geometry leads to a prominent Raman enhancement, which was further applied to molecular sensing. The R6G molecules on graphene microtubes can be detected even for a concentration as low as 10^{-11} M. We believe that this method can be a generalized way to realize the 3D tubular structure of other 2D materials.

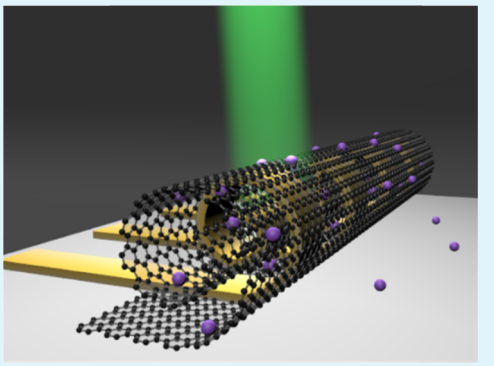

KEYWORDS: *monolayer graphene, microtube, Raman enhancement, molecular sensing*

INTRODUCTION

Graphene as the most promising two-dimensional (2D) material has exhibited extraordinary properties, such as special electronic structure, remarkable mechanical properties, and chemical inertness.[1−4] However, to exploit these properties for technological applications, inherently planar geometries are often required to be assembled into three-dimensional (3D) architectures.[5−7] Recently, various methods have been investigated to shape or construct planar mono/multilayer graphene into a 3D structure on a microscopic scale. Chen et al. have shown that the graphene nanostructure with fantastic properties can be fabricated through folding induced by an STM tip.[8] Although this method is precise, it is not suitable for large-scale fabrication. In most other investigations, rolling-up nanotechnology was used to create 3D structures of graphene. However, the atomically thin nature implies that graphene is too soft to support its weight, making it highly susceptible to destruction. As a result, in these reports, graphene had been laminated with other materials for self-support and protection. For example, Xu et al. showed a variety of 3D structures of graphene which is bonded to polydopamine and poly(*N*-isopropylacrylamide).[9] Mao et al. transferred graphene onto InGaAs/GaAs bilayers and obtained microtubes with the tube wall consisting of graphene/InGaAs/GaAs trilayers.[10] However, the incorporation inevitably affects the intrinsic properties of graphene.[11,12] Especially in the application of molecular sensors, the incorporation only allows one side of graphene to absorb molecules which largely reduces the absorption area. Moreover, massively charged impurities from a defective film or the dielectric mismatch between the graphene and other films can cover up the fluctuation induced by absorbed molecules leading to low sensitivity.[13] In previous studies, planar graphene has been used as a substrate for graphene-enhanced Raman scattering (GERS) to detect molecules in solution through the Raman test, which is quick and can provide structural information.[14] Compared with traditional noble metal-based substrates for surface-enhanced Raman scattering (SERS), the graphene substrate achieves stability, uniformity, and biocompatibility, which is supposed to be suitable for detecting biomolecules.[15] But the low Raman enhancement seriously limits its application.

In this work, monolayer graphene was successfully rolled into microtubes by depositing strain layers to provide driving force and support. Unlike previous reports where graphene needs to be incorporated with a much thicker layer, monolayer graphene grown on germanium substrate rolled up into microtubes under the drive of narrow chromium (Cr) stripes. Polycrystalline monolayer graphene grown on the Ge(111) substrate was used for its relatively moderate fracture toughness.[16,17] The diameter of the graphene microtubes can be tuned from 5.2 to 13.9 μm by changing the thickness of the

Received: July 4, 2021
Accepted: September 24, 2021

strain layers. Due to the suspension of the graphene as well as the tubular structure, large Raman enhancement was achieved.[18,19] To highlight the enhanced-Raman scattering of tubular graphene, the molecular sensors based on the GERS effect had been fabricated. Trace amounts of rhodamine 6G (R6G) molecules were detected down to 10^{-11} M showing excellent molecular sensing ability. Our work provides a new method to fabricate monolayer graphene microtubes which are anticipated to be applied to other 2D materials which may introduce unexpected applications or phenomena due to the special structure.

RESULTS AND DISCUSSION

Fabrication. The fabrication of the monolayer graphene microtubes is based on rolling-up nanotechnology.[20] First, polycrystalline monolayer graphene was grown on a 4-in. Ge(111) wafer through chemical vapor deposition.[21] Raman spectroscopy and atomic force microscopy (AFM) were applied to examine the quality of the as-grown graphene on Ge(111) substrate. Figure S1a shows the Raman spectra of graphene, in which the 2D to G peak ratio is larger than 1.5, confirming the monolayer feature of graphene, and the weak D peak comes from the grain boundary of the polycrystalline graphene.[22,23] The surface of the as-grown graphene is flat on the nanoscale. Note that, a few wrinkles that a generated during cooling in the CVD process due to thermal mismatch between graphene and Ge substrate are depicted by the red arrow in Figure S1b.[24] These wrinkles indicate the full coverage graphene on Ge substrate. Second, pre-strained Cr ribbons were deposited on the graphene using electron-beam evaporation as illustrated in Figure 1a. Cr was selected because its prestrain is controllable and large enough. In addition, Cr with good corrosion resistance can survive the following process of etching the Ge substrate. The interval of the Cr stripes (i.e., the width of the suspended graphene) is supposed to be small enough to avoid the destruction of graphene. Considering the requirement of following characterization and that the rolling path of Cr stripes is not completely straight, we set the interval of Cr stripes as 15 μm. The width of rectangular Cr stripes is also supposed to be small for preventing graphene from tearing and avoiding rolling from the long side.[25] Third, graphene was micropatterned through photolithography and reactive ion etching (RIE) as depicted in Figure 1b. The etch region is shown in Figure S2a. After that, the sample was transferred to a solution of HF(40%)−H_2O_2(40%)−H_2O (1:1:10) for etching the Ge substrate. The exposed Ge in the defined etch region was selectively etched. Once the graphene was released from the Ge substrate, it would roll up into a microtube driven by strain gradient in Cr ribbons as shown in Figure 1c. The process of forming the graphene microtubes in the etch solution was recorded by optical microscopy as displayed in Figure S2b−f. Finally, a critical point dryer was applied to avoid the collapse of the graphene microtube. The Cr microtubes serving as an inner framework of the microtube, are wrapped by the outer monolayer graphene. Between the Cr microtubes, monolayer graphene is suspended in the shape of a 3D microtube. To visualize the fabricated microtubes as well as the suspended graphene which is almost transparent in optical microscopy (Figure S3a), scanning electron microscopy (SEM) measurements were carried out. Figure 1d shows the top view of the fabricated 3D microtube, in which the Cr stripes are labeled by a golden color. Since graphene was suspended, the monolayer graphene microtube looks semitransparent which is consistent with previous reports.[26,27] The stereoscopic construction is more obvious in the side view with a tilt angle as shown in Figure S3b. In the side view, it can be clearly seen that the microtube rolled more than one circle, although the successive winds are not compact. Compared with other methods for rolling up graphene layers reported before, this was the first time that the tubular origami of monolayer graphene on the micrometer scale was realized.[9,28,29]

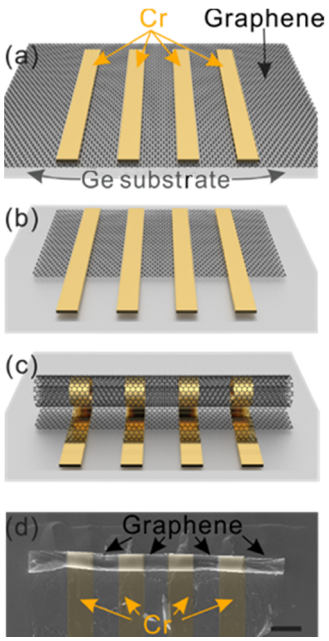

Figure 1. Fabrication and SEM images of rolled-up graphene microtubes. (a) Periodic strained Cr strips were deposited on graphene through electron-beam evaporation and lithography. (b) Defines the graphene pattern by lithography and RIE. (c) Ge underlayer was chemically etched by wet etching in diluted HF-H_2O_2 solution to trigger the self-rolling process. (d) Top view of a resulting graphene microtube on the Ge substrate. The scale bar is 20 μm.

The diameter of the rolled-up microtubes is mainly determined by the thickness and strain gradient of the multilayer film.[30,31] Due to the atomic thickness and extremely small out-of-plane stiffness of graphene, in the multilayer film, the prestrained Cr layers of several nanometers play a dominant role in controlling the diameter.[32] The strain gradient formed by the double Cr layers depends on the deposition conditions. The relaxed Cr layer was deposited at a low deposition rate, while the tensile strained Cr was deposited at a high deposition rate. Here, to tune the diameter of the rolled-up microtubes, we vary the thickness of Cr layers, but keep the deposition rate of the tensile strained Cr layer and the relaxed Cr layer unchanged. SEM images in Figure 2a show graphene microtubes with different diameters, ranging from 5.2 to 13.9 μm. For the flexibility of graphene, the suspended graphene crumpled, making it hard to define the diameter. In consequence, we take the average diameter of the inner Cr microtubes as the diameter of the graphene microtube. The tunability of the diameter is investigated in Figure 2b. The experimental data (red dots) show that the diameter increases with increasing total thickness which is equivalent to the sum of the thickness of the tensile Cr layer and the relaxed Cr layer. Based on the elastic mechanism and the plane strain

https://doi.org/10.1021/acsami.1c12592
ACS Appl. Mater. Interfaces XXXX, XXX, XXX−XXX

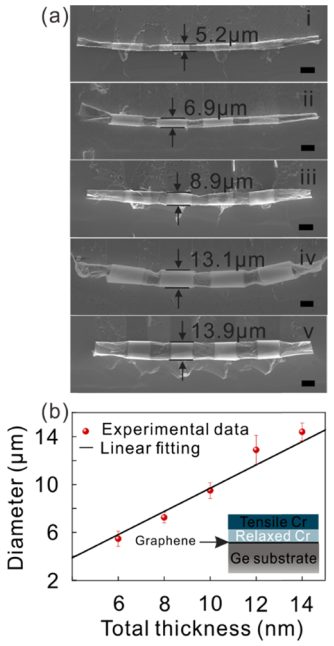

Figure 2. Diameter control of graphene microtubes. (a) SEM images of graphene microtubes with various diameters. The scale bars are 10 μm. (b) The relationship between the total thickness and the diameter. The inset shows the multilayer structure and the strain state of the Cr layer.

assumption, and because the thickness of each Cr layer is equal, the diameter of the graphene microtubes is proportional to the total thickness (detailed analysis can be found in the Supplementary Section V).[33] Therefore, a linear fitting was applied as the black line in Figure 2b. It is noted that compared with the experimental data of small diameter, the experimental data of large diameter deviate more from the fitted line. We attribute it to the gradual temperature increase of the substrate as the deposition continues, which can influence the strain of the deposited layer.[34] For a large diameter that means thicker Cr layers need to be deposited, the temperature of the substrate will increase significantly, which results in deviation at a large diameter.

Characterization. An array of as-fabricated graphene microtubes with a controlled rolling direction are displayed in Figure 3a demonstrating the potential for mass production. Figure 3b depicts an enlarged SEM image of the microtube labeled by the red dotted line in Figure 3a. Raman mapping along the axis of the microtube was measured using a 514 nm laser with a spot size of 2 μm. Figure 3c shows the Raman result of the microtube, in which the D, G, and 2D peaks can be recognized through color distribution. Due to the low yield of Raman scattering and the atomic thickness of graphene, the Raman signals of graphene are supposed to be weak without employing techniques for Raman enhancement.[18,35] However, with an air microcavity between suspended graphene and the substrate, its Raman intensity can be greatly enhanced by interference-enhanced Raman scattering (IERS).[36,37] Therefore, the Raman intensity of suspended graphene (red region in Figure 3b) is significantly larger than that of graphene on the Cr strip. Figure 3d shows a comparison between the Raman spectrum acquired from suspended graphene (red line) and graphene on Cr (black line). It is noted that the Raman signals of suspended graphene are more than 50 times larger than graphene on Cr and the D peak remains negligible implying high quality of graphene after the fabrication process. At the same time, the background of the Raman spectra for suspended graphene is considerably low, which facilitates the identification of characteristic peaks. A similar result can also be obtained when the Raman spectra of the suspended graphene and as-grown graphene on Ge were compared as illustrated in Figure S4. Thus, through an on-chip graphene microtube fabrication, dramatic Raman enhancement was achieved at the suspended graphene part.

Molecular Sensing. To investigate the performance of the graphene microtubes in molecular sensing, the graphene-enhanced Raman scattering (GERS) signals of graphene microtubes with different diameters were investigated using R6G probe molecules.[38,39] The R6G molecules were deposited on the graphene microtubes by soaking in the solution. As illustrated in Figure 4a, the deposited R6G molecules represented by purple spheres are scattered on the sample, and the Raman measurement was carried out under an excitation laser wavelength of 514 nm. Compared with graphene on substrate, double sides of suspended graphene of the microtubes could absorb the R6G molecules when it was soaked in the solution. To avoid the interference from the nonuniform distribution of R6G molecules, the Raman spectrum of GERS in the following was the averaged result of 10 different points. As shown in Figure 4b, the R6G molecules that are absorbed on both sides of graphene emit Raman signals under an excitation laser. This means that the enhanced surface area is doubled compared with graphene on the substrate. Moreover, for the microtube structure, the enhanced surface area can be further increased when the number of turns increased. Thus, stronger Raman signals of

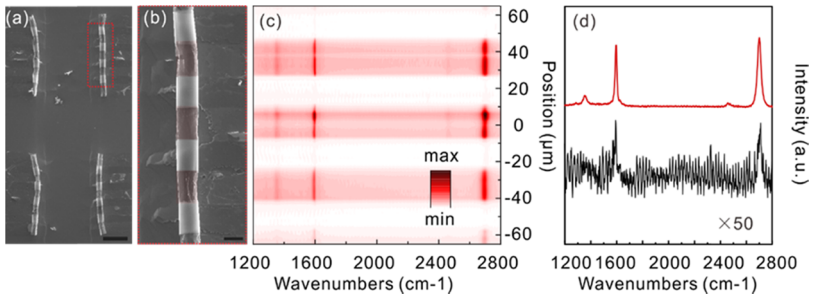

Figure 3. Characterization of rolling-up graphene microtubes. SEM images of the rolled-up graphene microtubes: (a) Array of microtubes, (b) an enlarged view of a microtube labeled by red dotted lines in (a), the suspended graphene region is highlighted in red color. (c) Raman mapping along the axis of the microtube in (b). (d) Raman spectrum for suspended graphene (red line) and graphene on Cr stripe (black line). The scale bars are equivalent to 50 μm in (a) and 10 μm in (b).

https://doi.org/10.1021/acsami.1c12592
ACS Appl. Mater. Interfaces XXXX, XXX, XXX−XXX

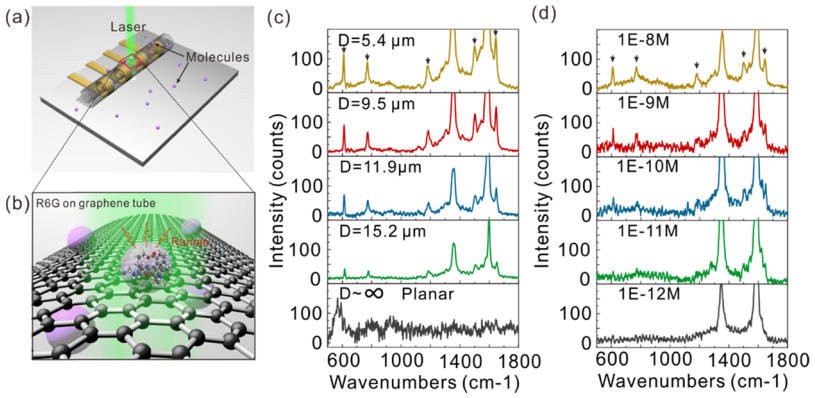

Figure 4. Performance of the GERS substrate based on graphene microtubes. (a, b) Schematic illustration of the Raman experiment for probing R6G molecules. (c) Raman spectra of R6G (8×10^{-9} M) on graphene microtubes with different diameters. (d) Raman spectra of R6G on graphene microtubes with similar diameters (~9.5 μm) as the R6G concentrations were reduced from 10^{-8} to 10^{-12} M. The peaks marked by the arrows are from R6G.

R6G molecules are supposed to be observed in the measured Raman spectrum, which exhibits better GERS performance. Graphene microtubes with different diameters were fabricated and soaked into the R6G solution at the same concentration. Raman signals at 610, 772, 1181, 1506, and 1647 cm^{-1} from R6G on graphene microtubes appeared as expected which are marked by the black arrows in Figure 4c. Because the substrate of R6G molecules is suspended graphene without any metal decoration, the Raman enhancement only comes from the chemical mechanism (CM).[40] A planar graphene on Ge that underwent the same process, was also measured under the same test conditions. In contrast with the graphene microtubes, there are no visible Raman peaks of R6G molecules. It is noted that the laser power we used here (1.5 mW) is lower than that used for the characterization of as-grown graphene (30 mW), as a consequence, the Raman peaks of planar graphene are also invisible. The Raman signal at around 580 cm^{-1} comes from the Ge substrate, but it disappears in the Raman spectrum of microtubes. This is because the focal plane of the laser was not near the Ge substrate when we test the Raman spectrum of the microtubes. In addition, as shown in Figure 4c, the intensity of Raman signals gradually increases as the diameter of graphene microtubes decreases. For clarification, Figure S5 shows the corresponding plot of the intensity of Raman peaks from R6G versus the diameter of microtubes which was extracted from Figure 4b. Obviously, the intensity of Raman signals can be enhanced by reducing the diameter of graphene microtubes. It is mainly attributed to the multilayer contribution. The number of turns increased as the diameter of graphene microtubes decrease. As a result, more layers of graphene with absorbed R6G molecules took part in the emission of Raman signals. Further investigations about the mechanism should be carried out in the future. To find out the detection limit for R6G molecules, graphene microtubes with a diameter of around 9.5 μm were chosen as GERS substrates. Then R6G solutions with five concentrations from 10^{-8} to 10^{-12} M were prepared. Figure 4d shows the enhanced Raman spectra of each R6G concentration for the graphene microtubes with similar diameters. It is obvious that the intensity of Raman signals of R6G molecules marked by black arrows decreases with decreasing concentration of the R6G solution. The Raman signals can even be recognized under concentrations as low as 10^{-11} M. The supercritical drying was carried out after transferring the samples into the R6G solution. The intermedia used in the critical point dryer is liquid CO_2 (99.999% purity), which is immiscible in the R6G solution, so it will not dilute the R6G solution after supercritical drying. In addition, as shown in Figure S6, when we used graphene on SiO_2 as a GERS substrate and a critical point dryer was also applied after soaking in the R6G solution, there are no Raman signals of R6G under a concentration of 10^{-10}, which is consistent with the previously reported result.[37] This means that the supercritical drying process will not condense the solution. Therefore, the interference caused by the supercritical drying process is eliminated. Table 1 summarizes the reported results of diverse GERS substrates applied in molecular sensing.[41−45] To the best of our knowledge, this is the first time that such low concentration (10^{-11} M for R6G) is detected using graphene or graphene derivatives as a substrate through the GERS effect. In addition, compared with other GERS substrates, the whole fabrication process of the graphene microtubes is CMOS compatible, which facilitates the practical application of GERS.

Table 1. Summary and Comparison of Molecular Sensing Performance of Various GERS Substrates

fabrication	type of graphene	detection level (M)	laser (nm)	reference
graphene on SiO_2/Si	exfoliated graphene	8×10^{-10}	514	41
graphene on SiO_2/Si	CVD N-doped graphene	1×10^{-8}	514	42
γ-Fe_2O_3/N-rGO composites	Hummers' method synthesized rGO	5×10^{-7}	532	43
graphene QDs on SiO_2/Si	PECVD GQDs	1×10^{-9}	532	44
feeding wrinkled graphene	CVD graphene	1×10^{-9}	533	45
rippled graphene on Au@Ag core nanopillars	CVD graphene	1×10^{-10}	633	46
monolayer graphene microtube	CVD graphene	1×10^{-11}	514	this work

CONCLUSIONS

In summary, we have transformed planar monolayer graphene into 3D tubular structures with different diameters through a

https://doi.org/10.1021/acsami.1c12592
ACS Appl. Mater. Interfaces XXXX, XXX, XXX−XXX

CMOS compatible rolling-up process. The diameter of graphene microtubes can be tuned by controlling the thickness of the strain layer, which is confirmed through experiments and theories. Benefiting from the suspension of the graphene and the 3D tubular structure, remarkable Raman enhancement was observed compared with planar graphene on the substrate. These graphene microtubes were then further used as a molecular sensor to probe R6G molecules through the GERS effect. The ultrasensitive sensing properties of the graphene microtubes showed that the R6G Raman signals can be detected at a concentration as low as 10^{-11} M. This efficient and versatile method to fabricate 3D tubular structure of graphene can be generalized to other 2D materials in the future.

EXPERIMENTAL SECTION

Device Fabrication. Large-area monolayer graphene was synthesized on Ge (111) wafer (415 μm thickness, AXT) using CH_4 as precursors in our AP-CVD system. The graphene sample was then spin-coated with a layer of photoresist (AZ5214) at 600 rpm for 6 s and 4000 rpm for 30 s. After that, the samples were baked on a hot plate at 90 °C for 90 s and a laser direct writer was utilized to define the pattern. The strain layers were then deposited on the graphene by e-beam evaporation (TSV70, Tenstar) under the following conditions: 25 °C temperature and 10^{-6} mbar vacuum pressure. The first Cr layer was deposited at a deposition rate of 0.2 Å s^{-1} and the second Cr layer was deposited at a deposition rate of 1 Å s^{-1} with same thickness of the first Cr layer. The interval of the Cr stripes is 15 μm and the widths of Cr strips are 15, 20, 25, and 30 μm. After the lift-off process in acetone solution, the second photolithography was performed to define the pattern of graphene. The exposed graphene was etched via RIE (Sirus T2) under the following condition: the O_2 gas flow of 35 sccm, reaction pressure of 165 mTorr, and the radio frequency power of 30 W. The photoresist was then dissolved in acetone solution. The etching window was defined by the photoresist through the third photolithography. Afterward, the sample was immersed in a solution of HF(40%)−H_2O_2(40%)−H_2O (1:1:10) to selectively etch the underlayer of Ge. Finally, the sample was transferred into a critical point dryer (CPD 030, Leica) to be dried, in which liquid CO_2 (99.999% purity) as an intermedia would gradually replace the initial acetone solution and then gasify at 40 °C.

Raman Measurement. The Raman spectrum was acquired using a micro-Raman spectroscope (HR800, Horiba) under ambient conditions. An excitation laser with a wavelength of 514 nm was focused onto the sample by a 100× objective lens and the laser spot size was about 1 μm. The laser power was adjusted to 1.5 mW when testing the graphene microtubes and 30 mW when testing the as-grown graphene on Ge.

Scanning Electron Microscopy. The morphologies of rolled-up graphene microtubes were characterized using a scanning electron microscope (HITACHI-S4700) with a 15 kV working voltage.

ASSOCIATED CONTENT

Supporting Information

The Supporting Information is available free of charge at https://pubs.acs.org/doi/10.1021/acsami.1c12592.

(S1) Characterization of as-grown graphene; (S2) optical images of the rolling-up process; (S3) optical image and SEM image of the fabricated graphene microtube; (S4) comparison of the Raman spectrum of the suspended graphene of graphene microtubes and graphene on Ge substrate; (S5) influence of the diameter on GERS performance; (S6) Raman spectrum of R6G on the Gr/SiO_2 substrate; and (Note) analysis of the relationship between the diameter and the total thickness (PDF)

AUTHOR INFORMATION

Corresponding Authors

Yongfeng Mei − *Department of Materials Science, State Key Laboratory of ASIC and Systems, Fudan University, Shanghai 200433, China;* orcid.org/0000-0002-3314-6108; Email: yfm@fudan.edu.cn

Zengfeng Di − *State Key Laboratory of Functional Materials for Informatics, Shanghai Institute of Microsystem and Information Technology, Chinese Academy of Sciences, Shanghai 200050, China;* orcid.org/0000-0002-9357-5107; Email: zfdi@mail.sim.ac.cn

Authors

Zhe Ma − *State Key Laboratory of Functional Materials for Informatics, Shanghai Institute of Microsystem and Information Technology, Chinese Academy of Sciences, Shanghai 200050, China; Center of Materials Science and Optoelectronics Engineering, University of Chinese Academy of Sciences, Beijing 100049, China;* orcid.org/0000-0001-7161-2539

Ziao Tian − *State Key Laboratory of Functional Materials for Informatics, Shanghai Institute of Microsystem and Information Technology, Chinese Academy of Sciences, Shanghai 200050, China*

Xing Li − *Department of Materials Science, State Key Laboratory of ASIC and Systems, Fudan University, Shanghai 200433, China*

Chunyu You − *Department of Materials Science, State Key Laboratory of ASIC and Systems, Fudan University, Shanghai 200433, China*

Yalan Wang − *State Key Laboratory of Functional Materials for Informatics, Shanghai Institute of Microsystem and Information Technology, Chinese Academy of Sciences, Shanghai 200050, China; Center of Materials Science and Optoelectronics Engineering, University of Chinese Academy of Sciences, Beijing 100049, China*

Complete contact information is available at: https://pubs.acs.org/10.1021/acsami.1c12592

Author Contributions

Z.T., Y.M., and Z.D. designed this study. Z.M. fabricated and characterized the devices. X.L. and C.Y. measured the properties. Z.M., Z.T., and Z.D. co-wrote the manuscript. All authors discussed the results and commented on the manuscript.

Notes

The authors declare no competing financial interest.

ACKNOWLEDGMENTS

This work is supported by the Science and Technology Commission of Shanghai Municipality (No. 17JC1401700), the Natural Science Foundation of China (Nos. 51322201, U1632115, 51602056, and 61905270), and the Natural Science Foundation of Shanghai (No. 19ZR1467100). Part of the experimental work has been carried out in Fudan Nanofabrication Laboratory. Part of the work was performed at the Center for Nanoscale Materials, a U.S. Department of Energy Office of Science User Facility, and supported by the U.S. Department of Energy, Office of Science, under Contract No. DE-AC02-06CH11357.

REFERENCES

(1) Novoselov, K. S.; Geim, A. K.; Morozov, S. V.; Jiang, D.; Zhang, Y.; Dubonos, S. V.; Grigorieva, I. V.; Firsov, A. A. Electric Field Effect in Atomically Thin Carbon Films. *Science* **2004**, *306*, 666−669.

(2) Lee, G. H.; Cooper, R. C.; An, S. J.; Lee, S.; van der Zande, A.; Petrone, N.; Hammerherg, A. G.; Lee, C.; Crawford, B.; Oliver, W.; Kysar, J. W.; Hone, J. High-Strength Chemical-Vapor Deposited Graphene and Grain Boundaries. *Science* **2013**, *340*, 1073−1076.

(3) Loh, K. P.; Bao, Q. L.; Ang, P. K.; Yang, J. X. The Chemistry of Graphene. *J. Mater. Chem.* **2010**, *20*, 2277−2289.

(4) Chen, J.; Walther, J. H.; Koumoutsakos, P. Strain Engineering of Kapitza Resistance in Few-Layer Graphene. *Nano Lett.* **2014**, *14*, 819−825.

(5) Chen, P. Y.; Liu, M. C.; Wang, Z. Y.; Hurt, R. H.; Wong, I. Y. From Flatland to Spaceland: Higher Dimensional Patterning with Two-Dimensional Materials. *Adv. Mater.* **2017**, *29*, No. 1605096.

(6) Deng, D. H.; Novoselov, K. S.; Fu, Q.; Zheng, N. F.; Tian, Z. Q.; Bao, X. H. Catalysis with Two-Dimensional Materials and Their Heterostructures. *Nat. Nanotechnol.* **2016**, *11*, 218−230.

(7) Chen, J.; Walther, J. H.; Koumoutsakos, P. Covalently Bonded Graphene-Carbon Nanotube Hybrid for High-Performance Thermal Interfaces. *Adv. Funct. Mater.* **2015**, *25*, 7539−7545.

(8) Chen, H.; Zhang, X. L.; Zhang, Y. Y.; Wang, D.; Bao, D. L.; Que, Y. D.; Xiao, W. D.; Du, S. X.; Ouyang, M.; Pantelides, S. T.; Gao, H. J. Atomically Precise, Custom-Design Origami Graphene Nanostructures. *Science* **2019**, *365*, 1036−1040.

(9) Xu, W. A.; Qin, Z.; Chen, C. T.; Kwag, H. R.; Ma, Q. L.; Sarkar, A.; Buehler, M. J.; Gracias, D. H. Ultrathin Thermoresponsive Self-Folding 3D Graphene. *Sci. Adv.* **2017**, *3*, No. e1701084.

(10) Mao, G. M.; Wang, Q.; Chai, Z. E.; Liu, H.; Liu, K.; Ren, X. M. Realization of Uniaxially Strained, Rolled-Up Monolayer CVD Graphene on a Si Platform via Heteroepitaxial InGaAs/GaAs Bilayers. *RSC Adv.* **2017**, *7*, 14481−14486.

(11) Berciaud, S.; Ryu, S.; Brus, L. E.; Heinz, T. F. Probing the Intrinsic Properties of Exfoliated Graphene: Raman Spectroscopy of Free-Standing Monolayers. *Nano Lett.* **2009**, *9*, 346−352.

(12) Freitag, M.; Low, T.; Avouris, P. Increased Responsivity of Suspended Graphene Photodetectors. *Nano Lett.* **2013**, *13*, 1644−1648.

(13) Sun, J.; Muruganathan, M.; Mizuta, H. Room Temperature Detection of Individual Molecular Physisorption Using Suspended Bilayer Graphene. *Sci. Adv.* **2016**, *2*, No. e1501518.

(14) Xu, W. G.; Ling, X.; Xiao, J. Q.; Dresselhaus, M. S.; Kong, J.; Xu, H. X.; Liu, Z. F.; Zhang, J. Surface Enhanced Raman Spectroscopy on a Flat Graphene Surface. *Proc. Natl. Acad Sci. U.S.A.* **2012**, *109*, 9281−9286.

(15) Chen, N.; Xiao, T. H.; Luo, Z.; Kitahama, Y.; Hiramatsu, K.; Kishimoto, N.; Itoh, T.; Cheng, Z. Z.; Goda, K. Porous Carbon Nanowire Array for Surface-Enhanced Raman Spectroscopy. *Nat. Commun.* **2020**, *11*, No. 4772.

(16) Zhang, P.; Ma, L. L.; Fan, F. F.; Zeng, Z.; Peng, C.; Loya, P. E.; Liu, Z.; Gong, Y. J.; Zhang, J. N.; Zhang, X. X.; Ajayan, P. M.; Zhu, T.; Lou, J. Fracture Toughness of Graphene. *Nat. Commun.* **2014**, *5*, No. 3782.

(17) Shekhawat, A.; Ritchie, R. O. Toughness and Strength of Nanocrystalline Graphene. *Nat. Commun.* **2016**, *7*, No. 10546.

(18) Lin, T. Y.; Lee, Y. C.; Lee, Y. W.; Chang, S. W.; Ma, D. L.; Lin, B. C.; Chen, H. L. Air Gap-Based Cavities Dramatically Enhance the True Intrinsic Spectral Signals of Suspended and Pristine Two-Dimensional Materials. *J. Phys. Chem. C* **2019**, *123*, 5667−5679.

(19) Agarwal, K.; Dai, C. H.; Joung, D.; Cho, J. H. Nano-Architecture Driven Plasmonic Field Enhancement in 3D Graphene Structures. *ACS Nano* **2019**, *13*, 1050−1059.

(20) Xu, C. H.; Pan, R. B.; Guo, Q. L.; Wu, X.; Li, G. J.; Huang, G. S.; An, Z. H.; Li, X. L.; Mei, Y. F. Ultrathin Silicon Nanomembrane in a Tubular Geometry for Enhanced Photodetection. *Adv. Opt. Mater.* **2019**, *7*, No. 1900823.

(21) Zheng, X. H.; Gao, L.; Yao, Q. Z.; Li, Q. Y.; Zhang, M.; Xie, X. M.; Qiao, S.; Wang, G.; Ma, T. B.; Di, Z. F.; Luo, J. B.; Wang, X. Robust Ultra-Low-Friction State of Graphene via Moire Superlattice Confinement. *Nat. Commun.* **2016**, *7*, No. 13204.

(22) Wang, T. B.; Li, P. L.; Hu, X. D.; Gao, M.; Di, Z. F.; Xue, Z. Y.; Zhang, M. Wafer-Scale Fabrication of Single-Crystal Graphene on Ge(110) Substrate by Optimized CH_4/H_2 Ratio. *Appl. Surf. Sci.* **2020**, *529*, No. 147066.

(23) Lee, J. H.; Lee, E. K.; Joo, W. J.; Jang, Y.; Kim, B. S.; Lim, J. Y.; Choi, S. H.; Ahn, S. J.; Ahn, J. R.; Park, M. H.; Yang, C. W.; Choi, B. L.; Hwang, S. W.; Whang, D. Wafer-Scale Growth of Single-Crystal Monolayer Graphene on Reusable Hydrogen-Terminated Germanium. *Science* **2014**, *344*, 286−289.

(24) Zhu, W. J.; Low, T.; Perebeinos, V.; Bol, A. A.; Zhu, Y.; Yan, H. G.; Tersoff, J.; Avouris, P. Structure and Electronic Transport in Graphene Wrinkles. *Nano Lett.* **2012**, *12*, 3431−3436.

(25) Chun, I. S.; Challa, A.; Derickson, B.; Hsia, K. J.; Li, X. Geometry Effect on the Strain-Induced Self-Rolling of Semiconductor Membranes. *Nano Lett.* **2010**, *10*, 3927−3932.

(26) Barcelos, I. D.; Moura, L. G.; Lacerda, R. G.; Malachias, A. Observation of Strain-Free Rolled-Up CVD Graphene Single Layers: Toward Unstrained Heterostructures. *Nano Lett.* **2014**, *14*, 3919−3924.

(27) Wang, H. D.; Hu, S. Q.; Takahashi, K.; Zhang, X.; Takamatsu, H.; Chen, J. Experimental Study of Thermal Rectification in Suspended Monolayer Graphene. *Nat. Commun.* **2017**, *8*, No. 15843.

(28) Teshima, T. F.; Henderson, C. S.; Takamura, M.; Ogawa, Y.; Wang, S. N.; Kashimura, Y.; Sasaki, S.; Goto, T.; Nakashima, H.; Ueno, Y. Self-Folded Three-Dimensional Graphene with a Tunable Shape and Conductivity. *Nano Lett.* **2019**, *19*, 461−470.

(29) Wang, L.; Tian, Z. A.; Zhang, B. R.; Xu, B. R.; Wang, T. B.; Wang, Y.; Li, S. L.; Di, Z. F.; Mei, Y. F. On-Chip Rolling Design for Controllable Strain Engineering and Enhanced Photon-Phonon Interaction in Graphene. *Small* **2019**, *324*, No. 1805477.

(30) Tian, Z.; Zhang, L.; Fang, Y. F.; Xu, B.; Tang, S. W.; Hu, N.; An, Z. H.; Zi, C.; Mei, Y. F. Deterministic Self-Rolling of Ultrathin Nanocrystalline Diamond Nanomembranes for 3D Tubular/Helical Architecture. *Adv. Mater.* **2017**, *29*, No. 1604572.

(31) Xu, B.; Zhang, X.; Tian, Z.; Han, D.; Fan, X.; Chen, Y.; Di, Z.; Qiu, T.; Mei, Y. Microdroplet-Guided Intercalation and Deterministic Delamination towards Intelligent Rolling Origami. *Nat. Commun.* **2019**, *10*, No. 5019.

(32) Wei, Y. J.; Wang, B. L.; Wu, J. T.; Yang, R. G.; Dunn, M. L. Bending Rigidity and Gaussian Bending Stiffness of Single-Layered Graphene. *Nano Lett.* **2013**, *13*, 26−30.

(33) Nikishkov, G. P. Curvature Estimation for Multilayer Hinged Structures with Initial Strains. *J. Appl. Phys.* **2003**, *94*, 5333−5336.

(34) Songmuang, R.; Deneke, C.; Schmidt, O. G. Rolled-Up Micro- and Nanotubes from Single-Material Thin Films. *Appl. Phys. Lett.* **2006**, *89*, No. 223109.

(35) Ling, X.; Zhang, J. Interference Phenomenon in Graphene-Enhanced Raman Scattering. *J. Phys. Chem. C* **2011**, *115*, 2835−2840.

(36) Metten, D.; Federspiel, F.; Romeo, M.; Berciaud, S. All-Optical Blister Test of Suspended Graphene Using Micro-Raman Spectroscopy. *Phys. Rev. Appl.* **2014**, *2*, No. 054008.

(37) Li, Q.; Zhang, X.; Jiang, D.; Shingaya, Y.; Tsuya, D.; Nakayama, T. Raman Intensity Oscillation of Graphene over Sio_2/Si Micro-Cavity. *Jpn. J. Appl. Phys.* **2020**, *59*, No. 028001.

(38) Xie, L. M.; Ling, X.; Fang, Y.; Zhang, J.; Liu, Z. F. Graphene as a Substrate to Suppress Fluorescence in Resonance Raman Spectroscopy. *J. Am. Chem. Soc.* **2009**, *131*, 9890.

(39) Xu, W. G.; Mao, N. N.; Zhang, J. Graphene: A Platform for Surface-Enhanced Raman Spectroscopy. *Small* **2013**, *9*, 1206−1224.

(40) Stiles, P. L.; Dieringer, J. A.; Shah, N. C.; Van Duyne, R. R. Surface-Enhanced Raman Spectroscopy. *Annu. Rev. Anal. Chem.* **2008**, *1*, 601−626.

(41) Ling, X.; Xie, L. M.; Fang, Y.; Xu, H.; Zhang, H. L.; Kong, J.; Dresselhaus, M. S.; Zhang, J.; Liu, Z. F. Can Graphene Be Used as a Substrate for Raman Enhancement? *Nano Lett.* **2010**, *10*, 553−561.

(42) Feng, S. M.; dos Santos, M. C.; Carvalho, B. R.; Lv, R. T.; Li, Q.; Fujisawa, K.; Elias, A. L.; Lei, Y.; Perea-Lopez, N.; Endo, M.; Pan,

https://doi.org/10.1021/acsami.1c12592
ACS Appl. Mater. Interfaces XXXX, XXX, XXX−XXX

M. H.; Pimenta, M. A.; Terrones, M. Ultrasensitive Molecular Sensor Using N-Doped Graphene through Enhanced Raman Scattering. *Sci. Adv.* **2016**, *2*, No. e1600322.
(43) Yang, L. N.; Hu, J. G.; He, L. L.; Tang, J.; Zhou, Y. C.; Li, J.; Ding, K. X. One-Pot Synthesis of Multifunctional Magnetic N-Doped Graphene Composite for SERS Detection, Adsorption Separation and Photocatalytic Degradation of Rhodamine 6G. *Chem. Eng. J.* **2017**, *327*, 694−704.
(44) Liu, D. H.; Chen, X. S.; Hu, Y. B.; Sun, T.; Song, Z. B.; Zheng, Y. J.; Cao, Y. B.; Cai, Z.; Cao, M.; Peng, L.; Huang, Y. L.; Du, L.; Yang, W. L.; Chen, G.; Wei, D. P.; Shen, A. T.; Wei, D. C. Raman Enhancement on Ultra-Clean Graphene Quantum Dots Produced by Quasi-Equilibrium Plasma-Enhanced Chemical Vapor Deposition. *Nat. Commun.* **2018**, *9*, No. 193.
(45) Chen, W.; Gui, X.; Zheng, Y.; Liang, B.; Lin, Z.; Zhao, C.; Chen, H.; Chen, Z.; Li, X.; Tang, Z. Synergistic Effects of Wrinkled Graphene and Plasmonics in Stretchable Hybrid Platform for Surface-Enhanced Raman Spectroscopy. *Adv. Opt. Mater.* **2017**, *5*, No. 1600715.
(46) Prasad, A.; Chaichi, A.; Mahigir, A.; Sahu, S. P.; Ganta, D.; Veronis, G.; Gartia, M. R. Ripple Mediated Surface Enhanced Raman Spectroscopy on Graphene. *Carbon* **2020**, *157*, 525−536.

https://doi.org/10.1021/acsami.1c12592
ACS Appl. Mater. Interfaces XXXX, XXX, XXX−XXX